

0371300 1481400 X-65 1-18-65

[REDACTED]

NASA TECHNICAL
MEMORANDUM



NASA TM X-1032

NASA TM X-1032

CLASSIFICATION CHANGED
UNCLASSIFIED
By Authority of 10 26 476 Date 8-28-70

EXPERIMENTAL INVESTIGATION OF
THE FLOW FIELD AND HEAT TRANSFER
OVER THE APOLLO-CAPSULE AFTERBODY
AT A MACH NUMBER OF 20

by Joseph G. Marvin and Marvin Kussoy

[REDACTED]

*Ames Research Center
Moffett Field, Calif.*

Declassified by authority of NASA
Classification Office, Notices No. 206-
Dated 15 OCT 1970

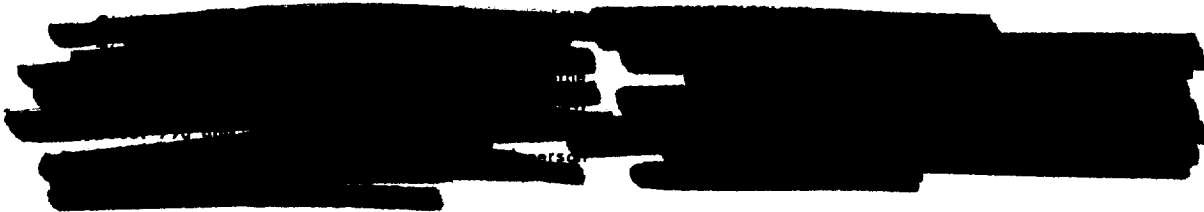
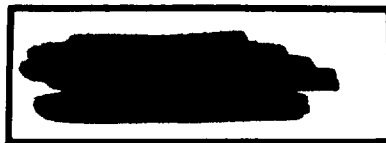
NATIONAL AERONAUTICS AND SPACE ADMINISTRATION • WASHINGTON, D. C. • FEBRUARY 1965

[REDACTED]

EXPERIMENTAL INVESTIGATION OF THE FLOW FIELD
AND HEAT TRANSFER OVER THE APOLLO-CAPSULE
AFTERBODY AT A MACH NUMBER OF 20

By Joseph G. Marvin and Marvin Kussoy

Ames Research Center
Moffett Field, Calif.



NATIONAL AERONAUTICS AND SPACE ADMINISTRATION

CONFIDENTIAL

11

RECEIVED

11

RECEIVED

11

RECEIVED

11

RECEIVED

[REDACTED]

EXPERIMENTAL INVESTIGATION OF THE FLOW FIELD
AND HEAT TRANSFER OVER THE APOLLO-CAPSULE
AFTERBODY AT A MACH NUMBER OF 20*

By Joseph G. Marvin and Marvin Kussoy

Ames Research Center
Moffett Field, Calif.

SUMMARY

Pressure and heat-transfer distributions, flow visualization photographs, and impact pressure surveys between the afterbody surface and the shock wave of a model of an Apollo capsule at angles of attack to 37.5° were obtained in helium at a Mach number of 20 and a free-stream Reynolds number based on maximum body diameter of 1.85×10^6 .

The flow over the most windward meridian of the afterbody surface changed from separated to attached between an angle of attack of 20° and 25° . For separated flows Prandtl-Meyer theory predicted the afterbody pressures when the initial slope of the flow separation boundary was known. Impact-pressure surveys were used to define the physical location of the separated boundary layer. The heating rate was adequately predicted by laminar flat-plate heat-transfer theory up to an angle of attack of 20° . For separated flow the heating rates were about one-half the calculated attached flow values. This agreed with Chapman's analysis for average heat transfer in regions of separated flows.

INTRODUCTION

Apollo forebody pressure and heat-transfer distributions in helium at $M_\infty = 20$ were reported in reference 1. As an extension of that work, afterbody pressures and heat transfer are presented herein and compared with theory. In addition, the results of flow visualization and impact-pressure surveys are presented and used to describe the afterbody flow.

SYMBOLS

h heat-transfer coefficient

M Mach number

*Title, Unclassified

[REDACTED]

p	pressure
q	heat-transfer rate
R	maximum radius of test body
S	distance along body surface from stagnation point at $\alpha = 0^\circ$
T	temperature
u	velocity
x	distance along reference line from forebody to probe position (see sketch in fig. 3)
y	vertical distance of the probe measured from reference line (see fig. 3)
α	angle of attack
ν	Prandtl-Meyer angle
ϕ	meridian angle with respect to vertical plane of symmetry (see fig. 1)

Subscripts

∞	condition in free stream
2	condition behind normal shock
o	stagnation condition at $\alpha = 0^\circ$
aw	adiabatic wall
e	condition at the edge of the boundary layer
s	shock wave
shoulder	condition existing at model shoulder
t	stagnation condition
w	condition at the wall



MODELS

The model and support configurations are shown in figure 1. Two models were used for pressure measurements and one for heat-transfer measurements. A solid brass model 2.5 inches in diameter with orifices of 0.036-inch diameter was used to measure pressures on the windward side of the body and for the oil-flow studies. For pressure tests on the leeward side of the body and for flow-field surveys, a model having a 2.0-inch diameter was used. A thin-skinned stainless-steel model 2.5 inches in diameter with a 0.017-inch average afterbody thickness was used for the heat-transfer tests.

INSTRUMENTATION


The afterbody pressures were recorded with bonded strain-gage pressure transducers with a differential range of 2 psia. The reference side of the cells was maintained at less than 50 microns pressure. Vibrating-diaphragm pressure transducers with a range of 0.2 psia were used during some of the tests as a check on the bonded strain-gage cells. The maximum error in afterbody pressure was ± 10 percent of the lowest pressures measured. The flow-field impact-pressure surveys were obtained with a bonded strain-gage pressure transducer with a differential range of 25 psia which was referenced to atmospheric pressure. The error in impact-pressure measurement varied from ± 20 percent of the separated-flow pressure to ± 5 percent of the inviscid-flow pressure. For the heat-transfer tests, chromel-constantan thermocouples were spot-welded to the interior of the afterbody skin. The error in temperature was $\pm 1^\circ$ F.

TEST FACILITY AND CONDITIONS

The tests were performed in the Ames 20-inch helium tunnel at $M_\infty = 20$. A description of this facility and operating conditions at $M_\infty = 20$ may be found in references 1 and 2. For the present tests the Reynolds number based on free-stream conditions and maximum body diameter was 1.85×10^6 . The reservoir stagnation temperature and pressure were about 530° R and 2000 psia, respectively.

TEST TECHNIQUE

The oil-flow and glow-discharge-flow visualization techniques described in references 1 and 3, respectively, were used in these tests. Briefly, the oil-flow technique consisted in painting the model with an emulsion of titanium dioxide, oleic acid, and vacuum-pump oil. The pattern that formed on the body remained after the flow was stopped. The model was removed from the test section and photographed. In the glow-discharge technique, a continuous



d-c voltage was applied across a cathode (the model) and an anode was placed above it and slightly downstream. Motion pictures were taken of the resulting glow discharge during the tests.

The technique used for the surface pressure tests is described in references 1 and 3. The flow-field survey data were obtained with a 0.010-inch inside diameter impact probe with a 0.007-inch wall thickness. This probe was positioned at or near the afterbody surface and moved through several vertical positions between the body and the shock wave. Only about five discrete points could be taken during a run because of the short test time and the time lag associated with the pressure transducer and tubing system. As a result, several test runs were required to complete a survey at each station.

The transient temperature technique was used for obtaining heat-transfer measurements. Heat transfer due to skin conduction was calculated and found to be negligible compared to the aerodynamic heat transfer. A possible exception to this was in the vicinity of the apex radius, where conduction errors could not be accurately calculated. The data are presented without conduction corrections.

REDUCTION OF DATA

All pressure data are presented as a ratio p/p_{t_2} where p is the local static pressure on the model or the local pitot pressure in the flow field and p_{t_2} is the total pressure measured with an impact probe located in the free stream.

The heat-transfer coefficient was obtained from experimental data by use of the following equation developed in reference 3:

$$\frac{q_w}{T_t p_t^{1/2}} = \frac{h}{p_t^{1/2}} \left(\frac{T_{aw}}{T_t} - \frac{T_w}{T_t} \right) \quad (1)$$

For each angle of attack, runs were made at several initial model wall temperatures T_w . Plots of T_w/T_t versus $q_w/T_t p_t^{1/2}$ were obtained, the slopes of which are proportional to the heat-transfer coefficient. The heat-transfer coefficient was normalized by the experimental value of h at the stagnation point at $\alpha = 0^\circ$ (see ref. 1). The error in these heat-transfer coefficients is estimated to be ± 10 percent.

RESULTS AND DISCUSSION

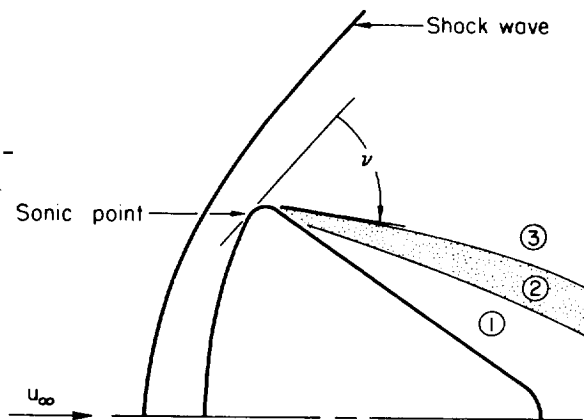
Flow Field

Flow visualization. - The flow around the Apollo afterbody was studied qualitatively by the two flow visualization techniques described earlier.

The results for the oil-flow technique are shown in figure 2(a). In this figure are front, plan-form, and side-view photographs of the model. The white lines trace the secondary flow within the boundary layer and thus indicate when the boundary layer is attached. Regions where definite line patterns do not appear have very low viscous shear and hence are believed to be adjacent to separated flow. The photographs suggest that the flow over the model is attached over the entire forebody and around the small corner radius for all angles of attack, but the exact line of flow separation is difficult to ascertain since it is probable that the actual line occurs somewhat upstream of the indicated line, as shown by the analysis in reference 4. The flow along the most windward meridian of the afterbody (see the plan-form photographs) was separated at small angles and attached at about $\alpha = 20^\circ$. The condition of the flow at various meridian plane angles can be observed in the side-view photographs; for example, the flow appears to be attached over almost all the windward half of the model at $\alpha = 33^\circ$.

Figure 2(b) presents photographs of the model and flow field at various angles of attack obtained by the glow-discharge technique. The light streaks emanating from the test body corner are attributed to the electrically excited gas within the boundary layer. The bright area above the model corner was caused by the anode probe above the model. Figure 2(b) suggests the flow over the windward surface of the afterbody changes from separated to attached at an angle of attack of 20° in agreement with the results indicated in figure 2(a). Also, it is recognized that the proximity of the anode probe to the region of interest may have disturbed the flow field in the wake region, but independent impact-probe measurements, discussed subsequently, tend to substantiate that the flow patterns of figure 2(b) are free of such disturbances.

The flow visualization photographs of figure 2 suggest a simplified model of the afterbody separated flow field. (See sketch (a).) The flow expands through an angle ν from the sonic point, around the corner, where the boundary layer separates and creates three regions in the afterbody flow field. Separated flow exists in region 1 and also probably reversed flow as concluded from tuft and injected oil-stream tests described in reference 5. Region 2 is the separated boundary layer. Region 3, from the outer edge of the boundary layer to the shock wave, is the inviscid flow field.



Sketch (a)

Impact-pressure surveys.— Flow-field surveys of impact pressure above the afterbody surface presented in figure 3 define the flow field just described. The sketch in this figure describes the coordinate system used. These surveys were taken at various distances downstream of the model forebody and at several angles of attack for the indicated meridian plane. The S/R locations are given whenever applicable. The different symbols represent

CONFIDENTIAL

data from different test runs. In general, for a given axial location, the impact pressure remains constant as the probe moves vertically away from the body surface (designated region 1 in fig. 3), increases very rapidly through the separated boundary layer (region 2), and then increases less rapidly in the inviscid-flow region (region 3).

The location of the separated boundary layer relative to the afterbody determined from the impact-survey data is presented graphically in figure 4. The symbols represent the inner and outer boundaries of region 2. The location of the separated boundary layer from the impact surveys (fig. 3) agrees so well with that indicated in figure 2(b) that it seems reasonable to conclude that the photographs of figure 2(b) do, in fact, reveal electrically excited gas within the boundary layer.

The data in figure 4 suggest an effect of angle of attack on the downstream growth of the separated boundary layer. This result may be influenced by misalignment of the probe with the local stream velocity, but to what extent is not presently known.

Pressure Distribution

Afterbody surface pressures are discussed and compared with theory. Figure 5 presents the normalized surface pressure p/p_{t_2} plotted against S/R for $\phi = 0^\circ$ at various angles of attack. Also shown are measured pressures for $\phi = 180^\circ$ at $\alpha = 33^\circ$. A small decrease in pressure takes place between 0° and 15° angle of attack and the pressure increases as the angle of attack is increased further to 20° , 25° , and 33° . An exception to this is the pressure at $S/R = 2.72$. The pressure at this S/R , the afterbody apex, remains practically unchanged with angle of attack and is believed to be the pressure in a region of separated flow. The leeward afterbody pressures at $\alpha = 33^\circ$ are constant and have the same magnitude as the $\alpha = 0^\circ$ data, indicating that these pressures are in the separated flow region.

The afterbody surface pressures were calculated by applying Prandtl-Meyer theory to the simplified flow-field model postulated and verified earlier (see sketch (a) and fig. 4). The flow-expansion angle ν was defined by the slope of the model surface at the sonic point and the initial slope of the outer edge of the separated boundary layer. For all angles of attack the slope of the model surface (relative to the free-stream direction) at the sonic point was assumed to be the tangent of 49° (a theoretical value at the sonic point on a hemisphere in high Mach number helium flow, see ref. 6). At angles of attack for which separated flow occurred the initial slope of the outer edge of the boundary layer was obtained either from the photographs in figure 2(b) or the impact surveys, and at values of α for attached flow the slope of the afterbody surface was employed. As shown in figure 5, Prandtl-Meyer theory adequately predicts the pressure for cases of separated flow ($\alpha = 0^\circ$ and $\alpha = 15^\circ$ for $\phi = 0^\circ$ and $\alpha = 33^\circ$ for $\phi = 180^\circ$). For cases of attached flow ($\alpha > 15^\circ$), Prandtl-Meyer theory does not adequately predict the afterbody pressures.

[REDACTED]

Also shown in figure 5 for $\alpha = 0^\circ$, 15° , and 33° is the static pressure at the outer edge of the separated boundary layer deduced from the flow-field surveys discussed earlier. A Mach number at the edge of the boundary layer was obtained from impact-pressure surveys assuming an isentropic expansion from the stagnation-point pressure. This Mach number was used for determining the ratio of static to total pressure at the edge of the boundary layer; this pressure is a little lower than the measured surface pressure.

Heat Transfer

It is of interest to examine the heat transfer to the afterbody in light of the afterbody flow field described in the previous sections. The distribution of the normalized heat-transfer coefficient for the windward afterbody surface at various angles of attack is plotted against S/R in figure 6. The data at $\alpha = 0^\circ$ represent the average for the three meridians. At $\alpha = 0^\circ$, a peak in the heat-transfer distribution occurs at $S/R = 2.62$. The photographs of figure 2(a) do not show any flow peculiarities which might explain an increase in heat transfer in this region. However, as demonstrated in reference 5, this peak is probably a result of sting interference effects. The first significant change in the heat-transfer distribution with ϕ takes place at $\alpha = 20^\circ$, the angle as deduced from figures 2(a) and 2(b) for flow attachment. With further increases in α , the heat-transfer variation with S/R changes along the $\phi = 0^\circ$ meridian, becoming highest near the model corner and decreasing toward the afterbody apex (a distribution typical of attached laminar flows). Note that the heat transfer along the $\phi = 90^\circ$ meridian as well as that at $S/R = 2.72$ remains essentially unchanged with increasing angle of attack. This result is characteristic of regions of separated flow, and is consistent in this respect with the photographs of figure 2(a).

The solid lines in figure 6 for $\alpha \geq 20^\circ$ represent calculations, using laminar flat-plate theory, of the heat-transfer coefficient distribution for attached flow along the windward meridian. (Details for applying this theory are presented in ref. 3.) In regions of flow separation ($\alpha = 0^\circ$ and $\alpha = 15^\circ$), the results from the theory were multiplied by 0.56, the ratio of average heat transfer for separated flow to that for attached flow as calculated in reference 7 and this method predicts the data quite well for angles of attack less than 20° .

CONCLUSIONS

A study of the flow field, surface pressure, and heating rates on the afterbody of the Apollo command module in helium at $M_\infty = 20$ resulted in the following conclusions:

[REDACTED]

[REDACTED]

1. The flow was definitely attached along the most windward surface for angles of attack greater than 20° and separated for angles of attack of 15° or less.

2. Impact-pressure surveys can be used to locate a separated boundary layer in the afterbody flow field.

3. For the separated flow condition, Prandtl-Meyer theory adequately predicted afterbody pressures when the flow separation angle was known.

4. The aerodynamic heating was predicted quite well up to $\alpha = 20^\circ$ by use of laminar flat-plate theory for heat transfer. In regions of separated flow this theory was adjusted by the ratio of average heat transfer for separated flow to that for attached flow given by Chapman.

Ames Research Center
National Aeronautics and Space Administration
Moffett Field, Calif., Sept. 21, 1964

REFERENCES

1. Marvin, Joseph, Tendeland, Thorval, and Kussoy, Marvin: Apollo Forebody Pressure and Heat-Transfer Distributions in Helium at $M_\infty = 20$. NASA TM X-854, 1963.
2. Tendeland, Thorval, and Pearson, Byrd D.: Effectiveness of Two Flap Controls on a Mercury Type Capsule at Mach Number of 15 in the Ames Hypersonic Helium Tunnel. NASA TM X-660, 1962.
3. Marvin, Joseph: Pressure and Heat-Transfer Distribution on the Afterbody of a Lifting Mercury-Type Capsule at Mach Number 15 in Helium. NASA TM X-783, 1963.
4. Squire, L. C.: The Motion of a Thin Oil Sheet Under the Boundary Layer on a Body. Royal Aircraft Establishment, Aero 2636, Feb. 1960.
5. Jones, Robert A.: Experimental Investigation of the Overall Pressure Distribution, Flow Field, and Afterbody Heat-Transfer Distribution of an Apollo Reentry Configuration at a Mach Number of 8. NASA TM X-813, 1963.
6. Van Dyke, Milton D., and Gordon, Helen, D.: Supersonic Flow Past a Family of Blunt Axisymmetric Bodies. NASA TR R-1, 1959.
7. Chapman, Dean R.: A Theoretical Analysis of Heat Transfer in Regions of Separated Flow. NACA TN 3792, 1956.

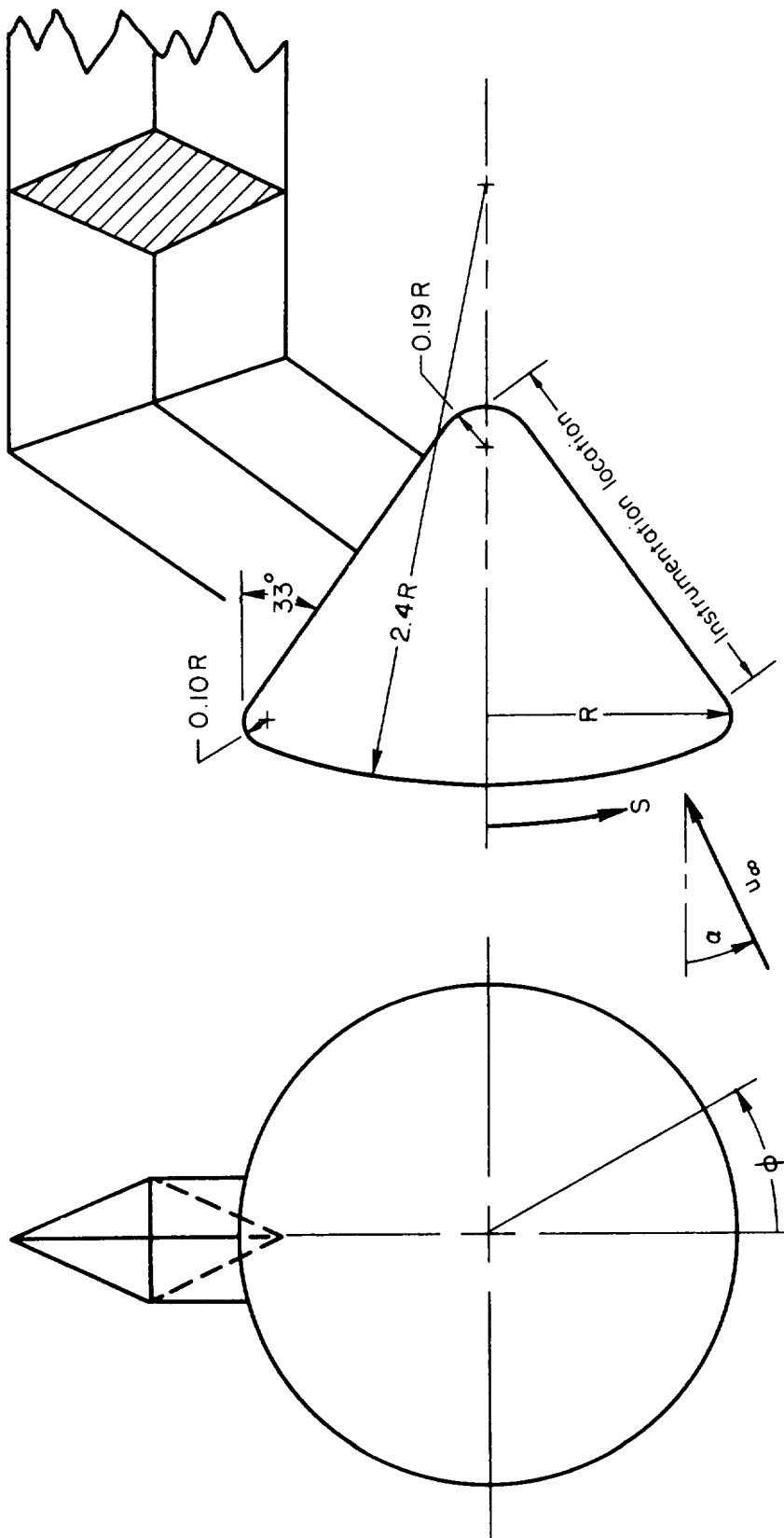
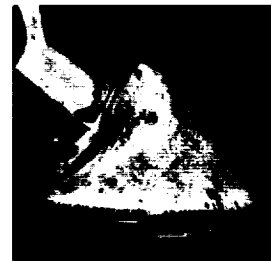
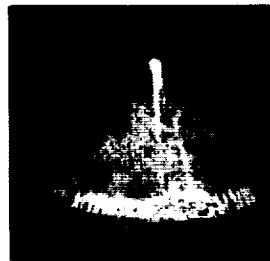
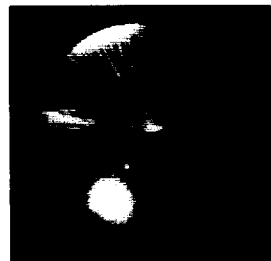


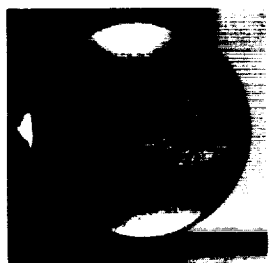
Figure 1.- Test model configuration.



$\alpha = 0^\circ$



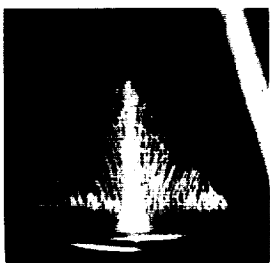
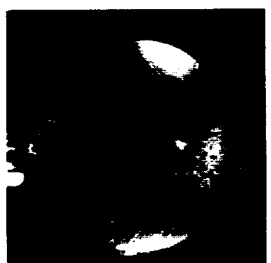
$\alpha = 15^\circ$



$\alpha = 20^\circ$
Side view

Front view

Plan view



$\alpha = 25^\circ$



$\alpha = 33^\circ$

A-30816, 1

(a) Oil-flow patterns.

Figure 2.- Flow-visualization photographs.



$\alpha = 0^\circ$



$\alpha = 15^\circ$



$\alpha = 20^\circ$



$\alpha = 25^\circ$

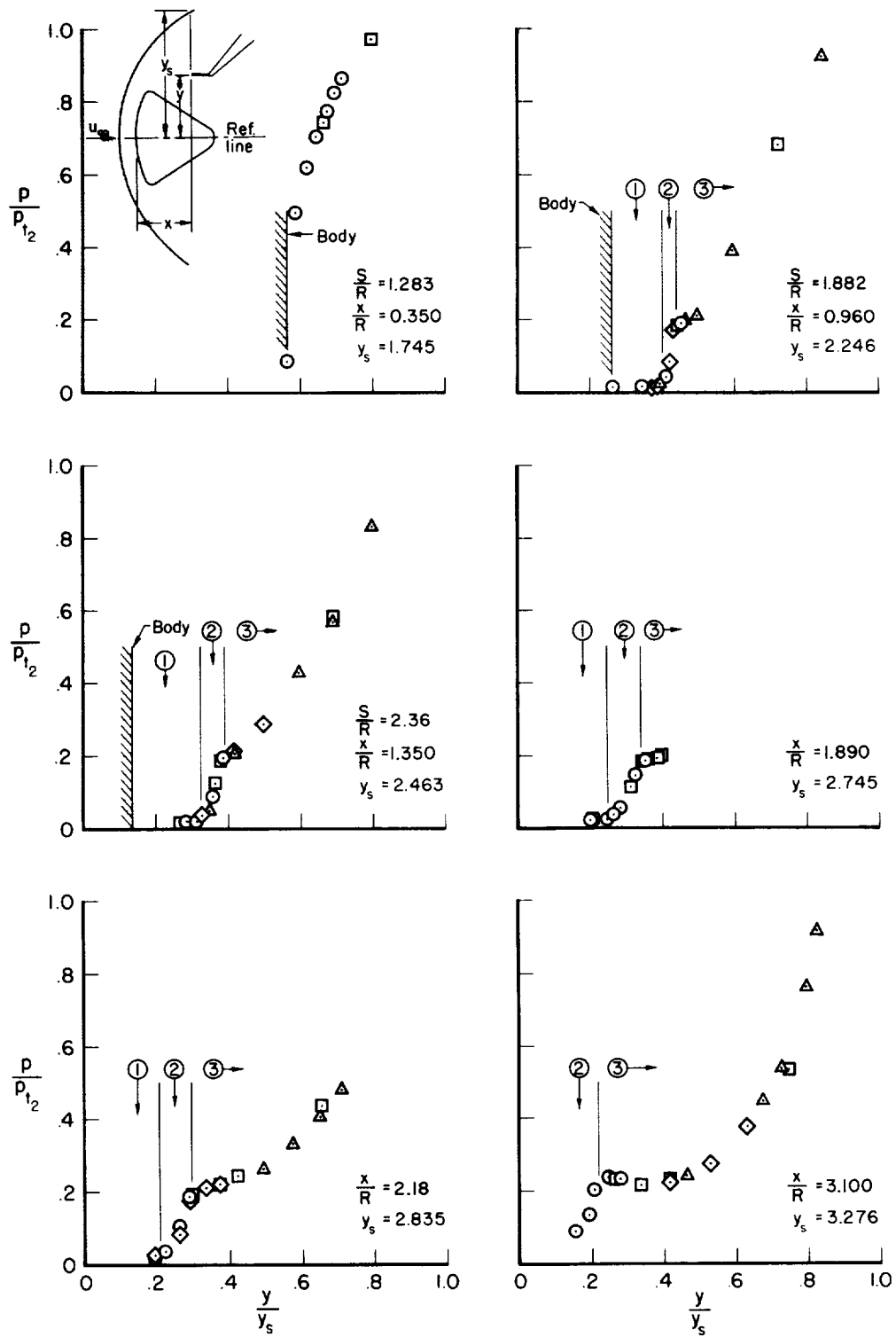


$\alpha = 33^\circ$

A-31443

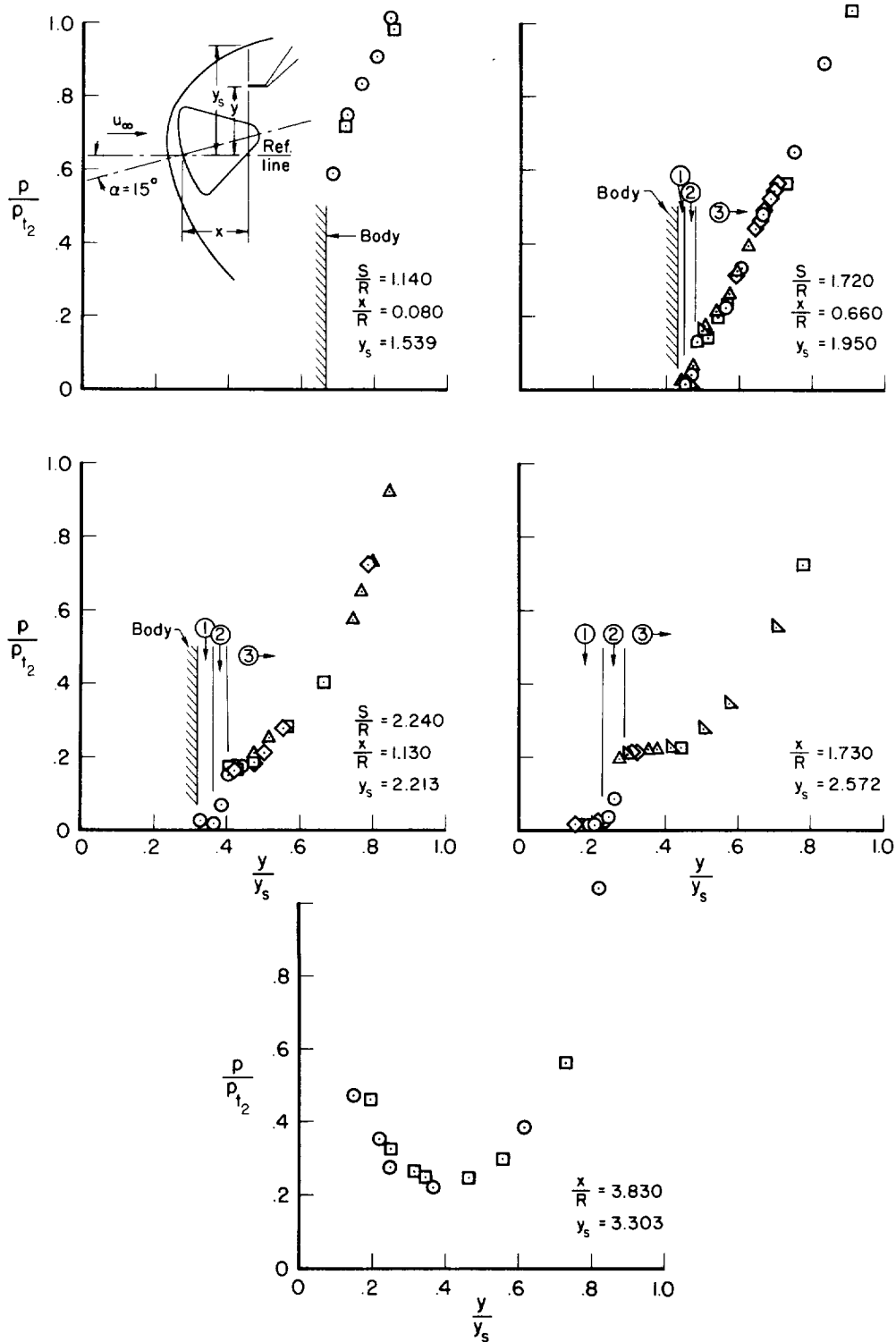
(b) Glow-discharge patterns.

Figure 2.- Concluded.



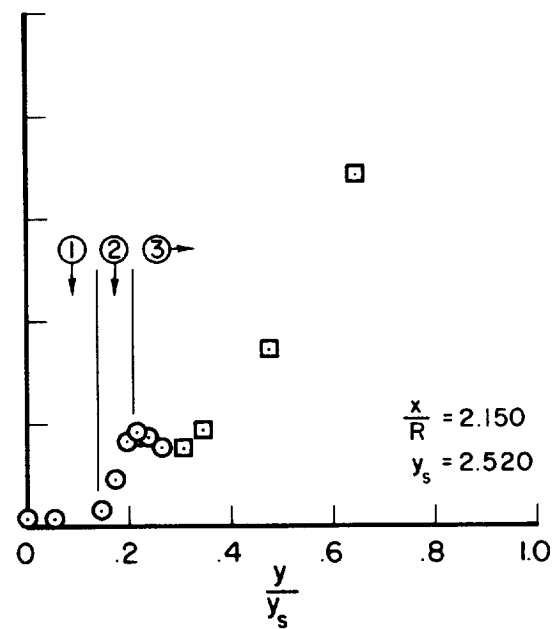
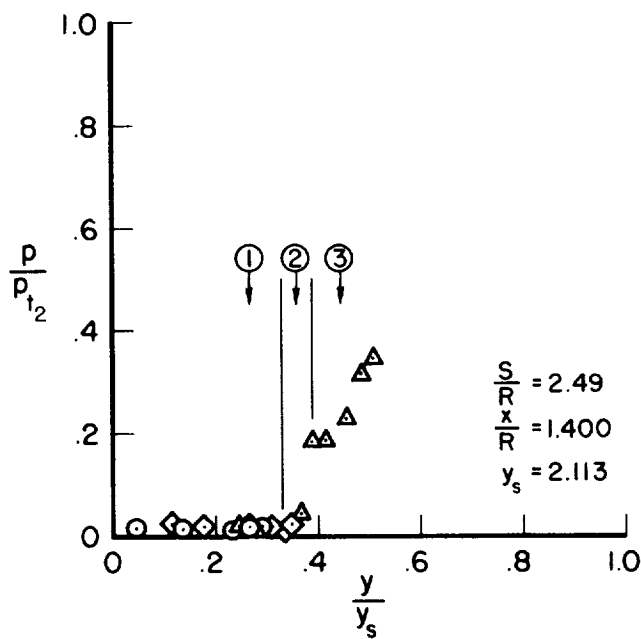
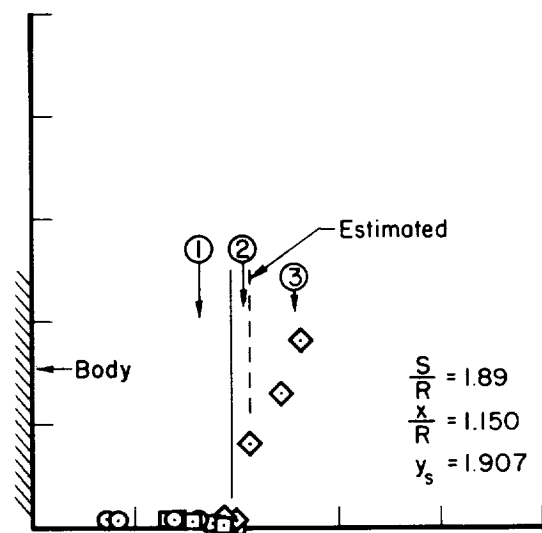
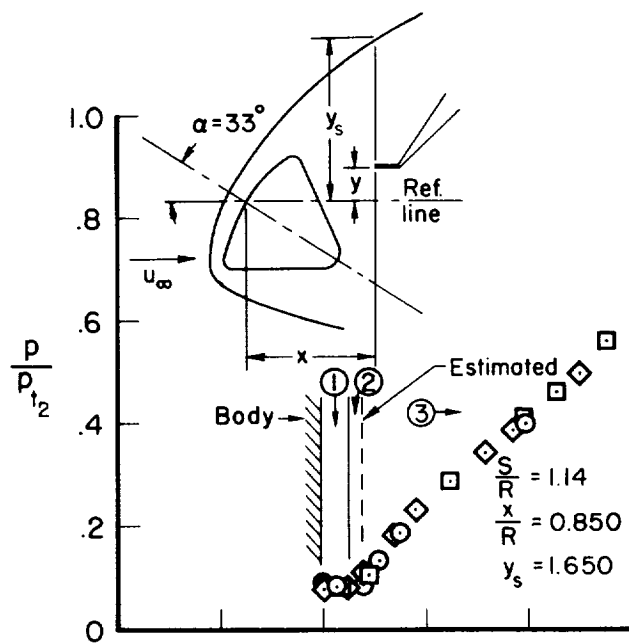
(a) $\alpha = 0^\circ$, $\phi = 0^\circ$

Figure 3.- Typical flow-field surveys over the Apollo afterbody.



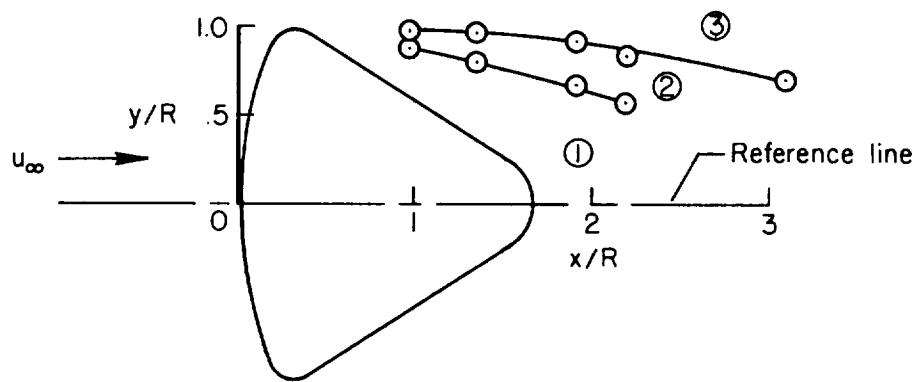
(b) $\alpha = 15^\circ$, $\varphi = 0^\circ$

Figure 3.- Continued.

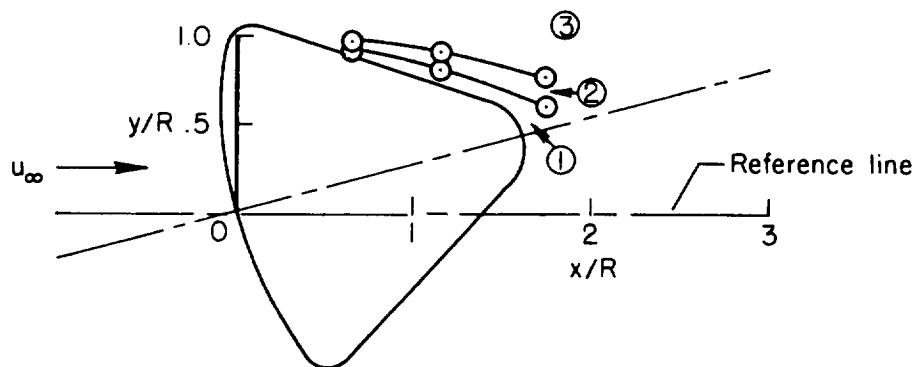


(c) $\alpha = 33^\circ$, $\varphi = 180^\circ$

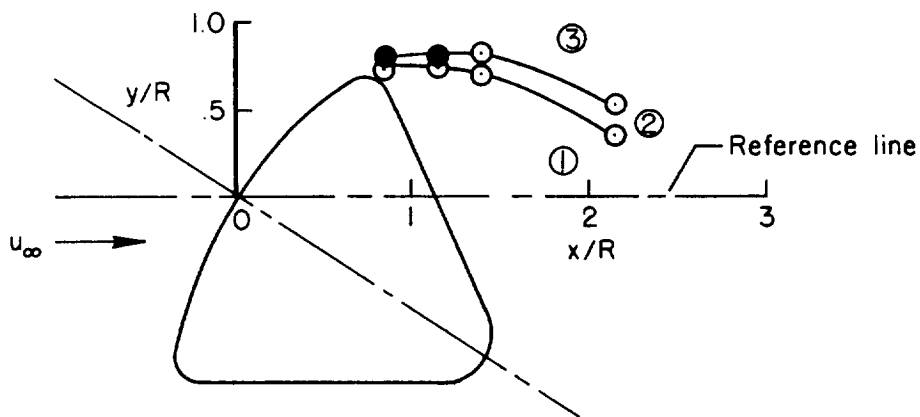
Figure 3.- Concluded.



(a) $\alpha = 0^\circ$, $\phi = 0^\circ$

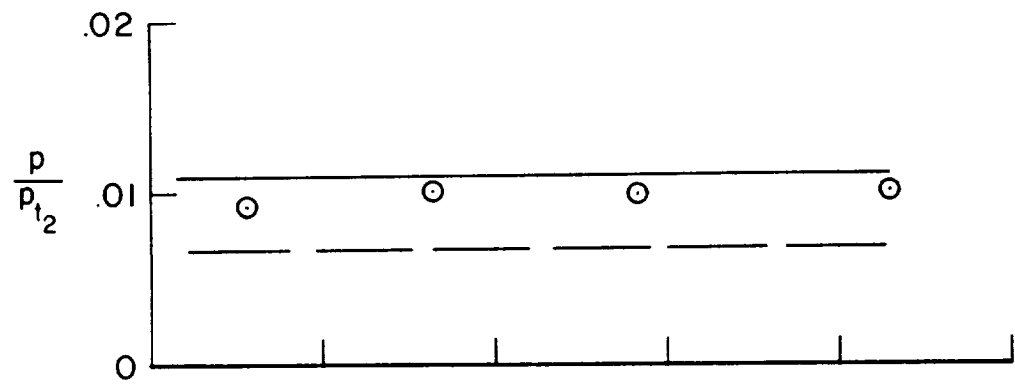


(b) $\alpha = 15^\circ$, $\phi = 0^\circ$

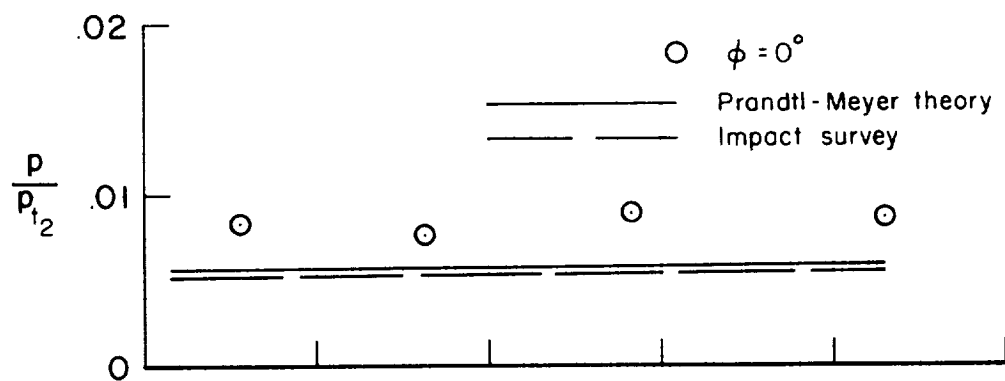


(c) $\alpha = 33^\circ$, $\phi = 180^\circ$

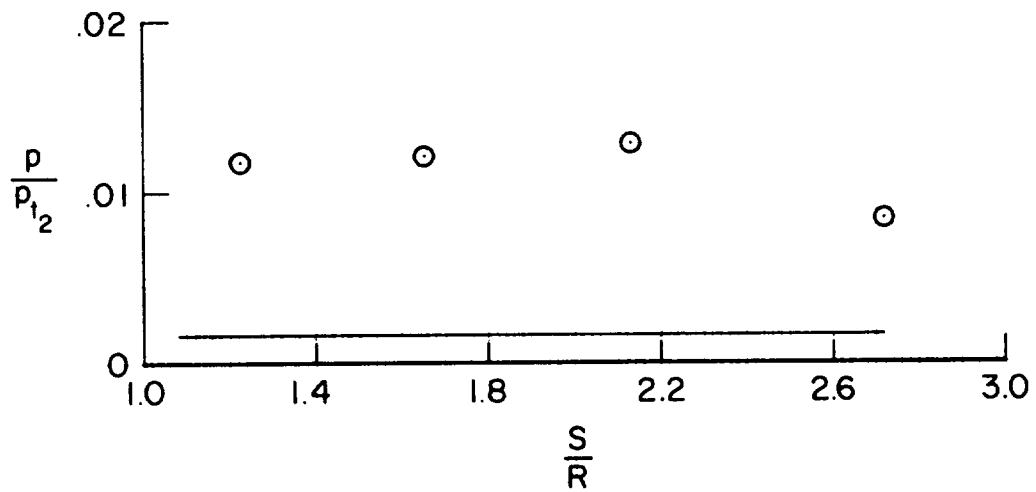
Figure 4.- Location of the separated boundary layer relative to the Apollo afterbody.



(a) $\alpha = 0^\circ$



(b) $\alpha = 15^\circ$



(c) $\alpha = 20^\circ$

Figure 5.- Distribution of surface pressure on Apollo afterbody.

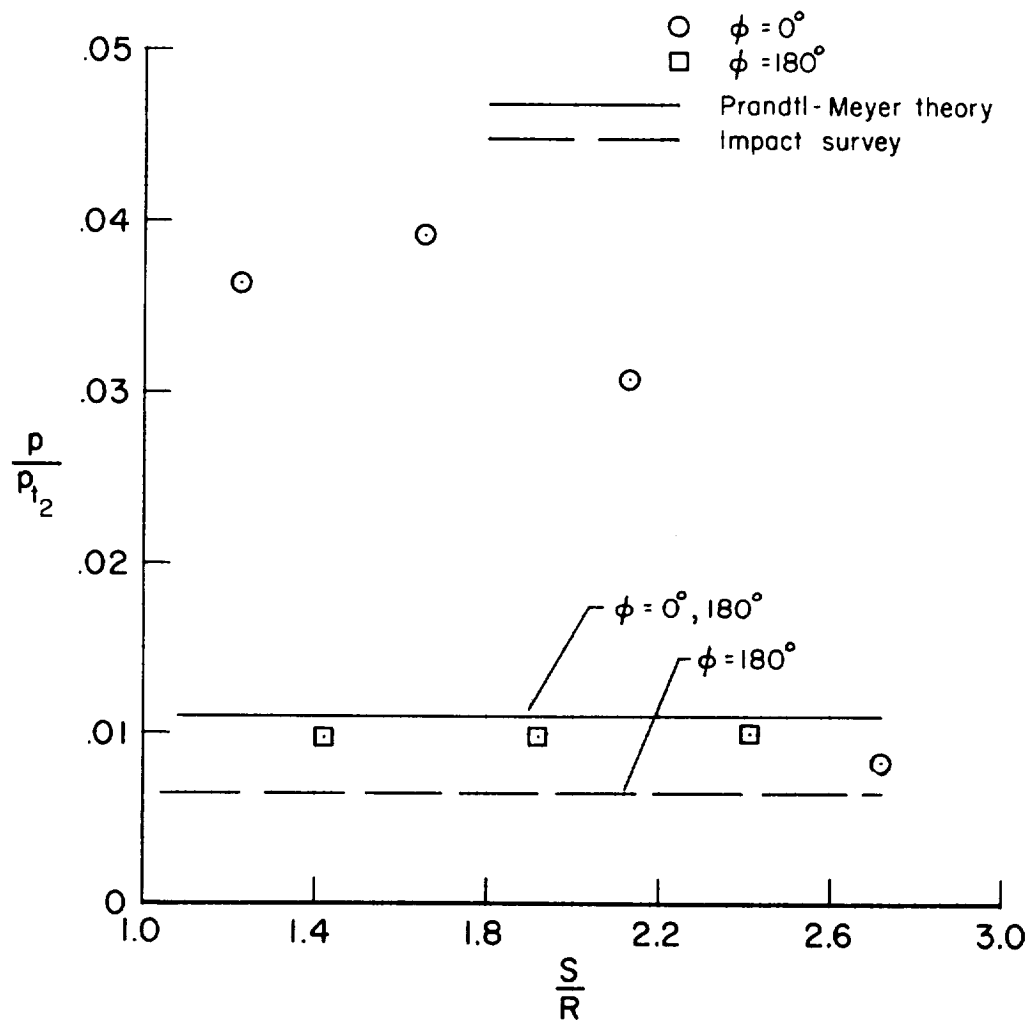
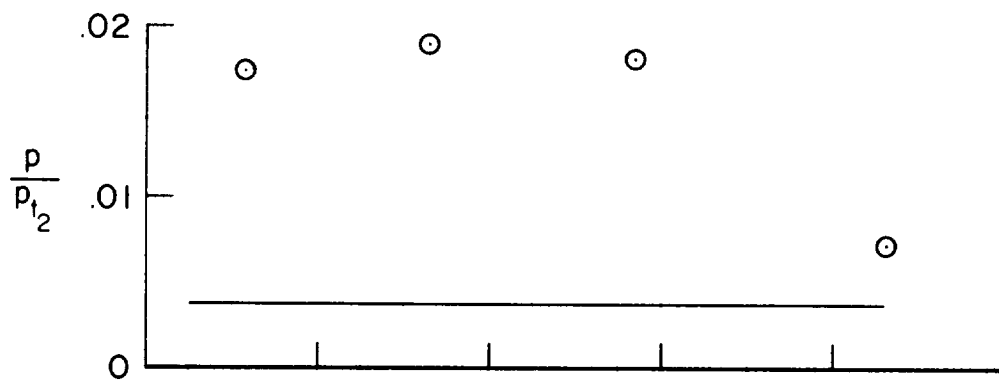
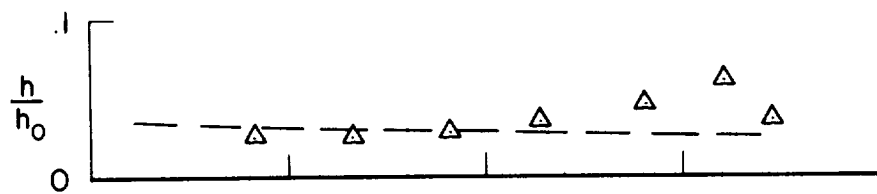
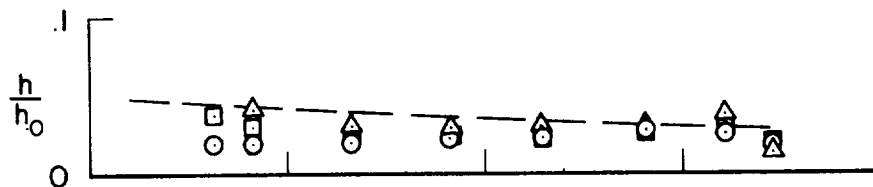


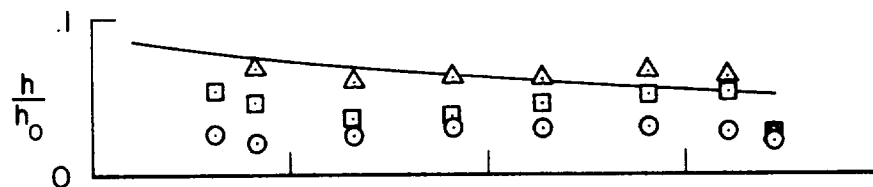
Figure 5.- Concluded.



(a) $\alpha = 0^\circ$

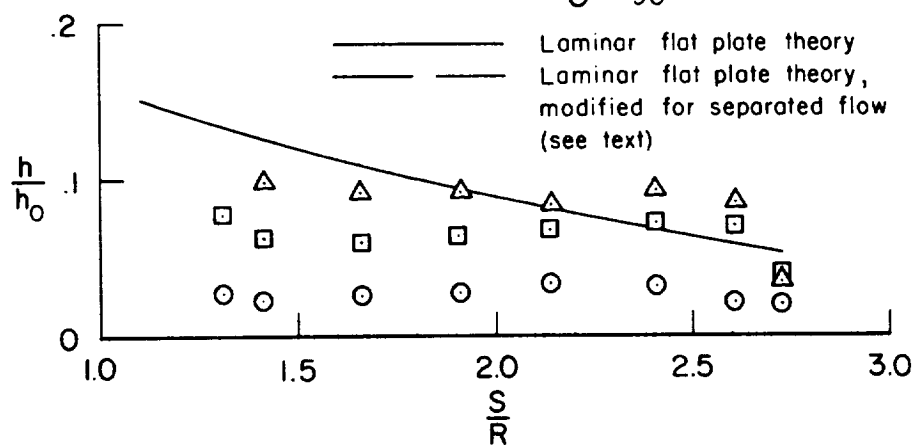


(b) $\alpha = 15^\circ$



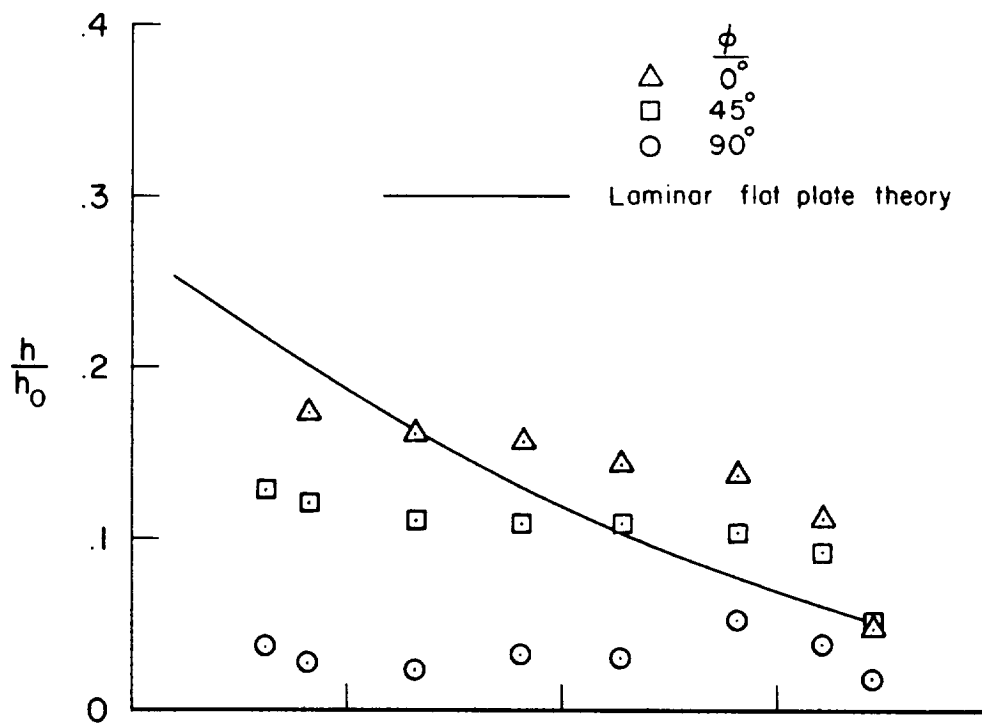
(c) $\alpha = 20^\circ$

ϕ
 \triangle 0°
 \square 45°
 \circ 90°

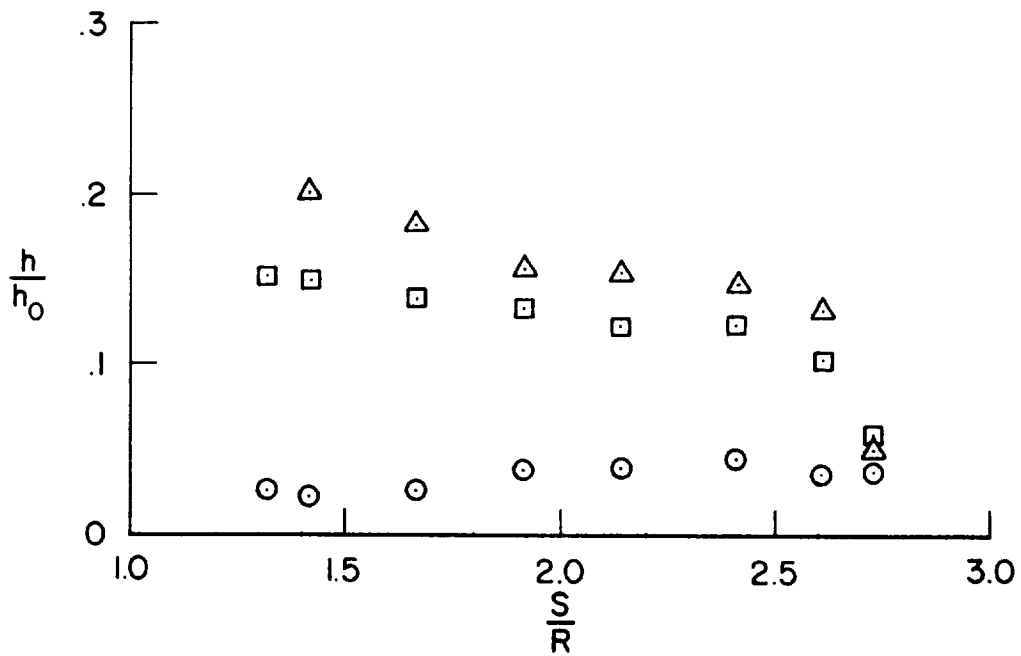


(d) $\alpha = 25^\circ$

Figure 6.- Distribution of normalized heat-transfer coefficient on afterbody surface of Apollo.

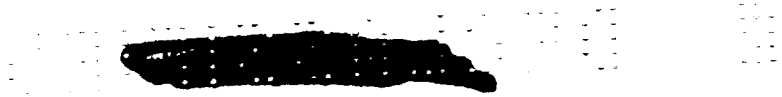


(e) $\alpha = 33^\circ$



(f) $\alpha = 37.5^\circ$

Figure 6.- Concluded.



11

DECLASSIFIED

<p>NASA TM X-1032 THIS CARD UNCLASSIFIED National Aeronautics and Space Administration. EXPERIMENTAL INVESTIGATION OF THE FLOW FIELD AND HEAT TRANSFER OVER THE APOLLO- CAPSULE AFTERBODY AT A MACH NUMBER OF 20. Joseph G. Marvin and Marvin Kussoy. February 1965. 19p. (NASA TECHNICAL MEMORANDUM X-1032) (REPORT CONFIDENTIAL)</p> <p>The description of the flow over the Apollo afterbody is substantiated by flow visualization photographs, impact-pressure surveys between the afterbody surface and the shock wave, and by surface pressure and heat-transfer distributions. These were obtained in helium at a free-stream Reynolds number of 1.85×10^6 based on maximum body diameter.</p>	<p>I. Marvin, Joseph G. II. Kussoy, Marvin III. NASA TM X-1032</p> <div> <p>GROUP 4</p> <p>Downgraded at 3 year intervals; declassified after 12 years</p> </div> <p>THIS CARD UNCLASSIFIED NASA</p>
<p>NASA TM X-1032 THIS CARD UNCLASSIFIED National Aeronautics and Space Administration. EXPERIMENTAL INVESTIGATION OF THE FLOW FIELD AND HEAT TRANSFER OVER THE APOLLO- CAPSULE AFTERBODY AT A MACH NUMBER OF 20. Joseph G. Marvin and Marvin Kussoy. February 1965. 19p. (NASA TECHNICAL MEMORANDUM X-1032) (REPORT CONFIDENTIAL)</p> <p>The description of the flow over the Apollo afterbody is substantiated by flow visualization photographs, impact-pressure surveys between the afterbody surface and the shock wave, and by surface pressure and heat-transfer distributions. These were obtained in helium at a free-stream Reynolds number of 1.85×10^6 based on maximum body diameter.</p>	<p>I. Marvin, Joseph G. II. Kussoy, Marvin III. NASA TM X-1032</p> <div> <p>GROUP 4</p> <p>Downgraded at 3 year intervals; declassified after 12 years</p> </div> <p>THIS CARD UNCLASSIFIED NASA</p>
<p>NASA TM X-1032 THIS CARD UNCLASSIFIED National Aeronautics and Space Administration. EXPERIMENTAL INVESTIGATION OF THE FLOW FIELD AND HEAT TRANSFER OVER THE APOLLO- CAPSULE AFTERBODY AT A MACH NUMBER OF 20. Joseph G. Marvin and Marvin Kussoy. February 1965. 19p. (NASA TECHNICAL MEMORANDUM X-1032) (REPORT CONFIDENTIAL)</p> <p>The description of the flow over the Apollo afterbody is substantiated by flow visualization photographs, impact-pressure surveys between the afterbody surface and the shock wave, and by surface pressure and heat-transfer distributions. These were obtained in helium at a free-stream Reynolds number of 1.85×10^6 based on maximum body diameter.</p>	<p>I. Marvin, Joseph G. II. Kussoy, Marvin III. NASA TM X-1032</p> <div> <p>GROUP 4</p> <p>Downgraded at 3 year intervals; declassified after 12 years</p> </div> <p>THIS CARD UNCLASSIFIED NASA</p>
<p>NASA TM X-1032 THIS CARD UNCLASSIFIED National Aeronautics and Space Administration. EXPERIMENTAL INVESTIGATION OF THE FLOW FIELD AND HEAT TRANSFER OVER THE APOLLO- CAPSULE AFTERBODY AT A MACH NUMBER OF 20. Joseph G. Marvin and Marvin Kussoy. February 1965. 19p. (NASA TECHNICAL MEMORANDUM X-1032) (REPORT CONFIDENTIAL)</p> <p>The description of the flow over the Apollo afterbody is substantiated by flow visualization photographs, impact-pressure surveys between the afterbody surface and the shock wave, and by surface pressure and heat-transfer distributions. These were obtained in helium at a free-stream Reynolds number of 1.85×10^6 based on maximum body diameter.</p>	<p>I. Marvin, Joseph G. II. Kussoy, Marvin III. NASA TM X-1032</p> <div> <p>GROUP 4</p> <p>Downgraded at 3 year intervals; declassified after 12 years</p> </div> <p>THIS CARD UNCLASSIFIED NASA</p>

"The aeronautical and space activities of the United States shall be conducted so as to contribute . . . to the expansion of human knowledge of phenomena in the atmosphere and space. The Administration shall provide for the widest practicable and appropriate dissemination of information concerning its activities and the results thereof."

—NATIONAL AERONAUTICS AND SPACE ACT OF 1958

NASA SCIENTIFIC AND TECHNICAL PUBLICATIONS

TECHNICAL REPORTS: Scientific and technical information considered important, complete, and a lasting contribution to existing knowledge.

TECHNICAL NOTES: Information less broad in scope but nevertheless of importance as a contribution to existing knowledge.

TECHNICAL MEMORANDUMS: Information receiving limited distribution because of preliminary data, security classification, or other reasons.

CONTRACTOR REPORTS: Technical information generated in connection with a NASA contract or grant and released under NASA auspices.

TECHNICAL TRANSLATIONS: Information published in a foreign language considered to merit NASA distribution in English.

TECHNICAL REPRINTS: Information derived from NASA activities and initially published in the form of journal articles.

SPECIAL PUBLICATIONS: Information derived from or of value to NASA activities but not necessarily reporting the results of individual NASA-programmed scientific efforts. Publications include conference proceedings, monographs, data compilations, handbooks, sourcebooks, and special bibliographies.

Details on the availability of these publications may be obtained from:

SCIENTIFIC AND TECHNICAL INFORMATION DIVISION
NATIONAL AERONAUTICS AND SPACE ADMINISTRATION

Washington, D.C. 20546